Materials Science & Engineering A 849 (2022) 143355

Contents lists available at ScienceDirect

Materials Science & Engineering A

journal homepage: www.elsevier.com/locate/msea

A novel sequential mechanism associated with stress-induced β→ω→β+α phase transformation in Ti–6Mo-3.5Cr–1Zr titanium alloy

Kai Chen [a], Qunbo Fan [a,b], Lin Yang [a,b,*], Shun Xu [a,b], Jiahao Yao [a,b], Yu Gao [a], Wei Lei [a]

[a] *National Key Laboratory of Science and Technology on Materials Under Shock and Impact, School of Materials Science and Engineering, Beijing Institute of Technology, Beijing, 100081, China*
[b] *Beijing Institute of Technology Chongqing Innovation Center, Chongqing, 401135, China*

ARTICLE INFO

Keywords:
Titanium alloy
Phase transformation
Microstructure
Stress-induced ω phase transformation

ABSTRACT

A novel metastable β-type Ti–6Mo-3.5Cr–1Zr alloy is designed using d-electrons theory to introduce diverse phase transformations. Stress-induced ω (SIω) phase transformation dominates the initial deformation, while the SIω bands are transformed to α+β phase as the strain increases. The sequential mechanism associated with β→SIω→α+β is first reported in titanium alloys.

1. Introduction

Since first discovered in Ti–8Cr (wt. %) alloy by Frost et al. [1], ω phase had received extensive attention due to its various morphologies and diverse phase transformation mechanisms associated with complex kinetic and thermodynamic formation processes, contributing to significant effects on mechanical properties.

The precipitation of ω phase from the β phase has been demonstrated to happen by the collapse of the (111) plane. The lattice of ω phase transforms from a trigonal structure to a hexagonal structure with the increasing degree of collapse [2,3]. According to the formation paths, the ω phase in titanium alloys can be classified into three categories: athermal ω phase [4,5], isothermal ω phase [6] and stress-induced ω (SIω) phase [7,8]. The first two types are dispersedly distributed in the β matrix. Their formation usually leads to an increase in the strength and a significant decrease in the ductility [9,10]. It has been experimentally observed that athermal ω phase can transform into β and α phases under external loading or thermal conditions. The ω-free dislocation channels were found in Ti–Nb alloys due to the athermal ω→β phase transformation, which confines the dislocation slips to localized regions and thus induces the brittleness of the alloy [11]. In addition, ω phase can assist the nucleation of α phase. The aging transition temperature of ω→α is experimentally determined between 300 °C and 500 °C [12–15]. The SIω phase transformation usually generates a band-like microstructure, creating transformation induced plasticity (TRIP) effect and thereby improving mechanical properties of the material [16–18]. Besides, its formation often accompanies with the generation of {112}<111> β twins due to their similar atomic shear [19], resulting in the zigzag configuration of {112}<111> β twin and SIω phase [20].

In this work, Ti–6Mo-3.5Cr–1Zr (wt. %) alloy was designed based on the d-electrons theory [21,22]. The alloy composition was pinpointed close to the ω phase transformation region in the *d* orbital level - bond order (Md-Bo) map: $Md = 2.399$, $Bo = 2.802$. The as-quenched alloy undergoes a series of stress-induced microstructure transformations during quasi-static tension. Interestingly, a novel sequential phase transition associated with β→SIω→(β+α) is reported for the first time. The underlying transformation mechanism is analyzed in details.

2. Material and methods

The experimental alloy was cast via vacuum arc smelting for three times. The contents of metallic elements were analyzed via an inductively coupled plasma optical emission spectrometer (ICP-OES, Agilent 730). The O, N and H concentrations were determined by an ONH-3000 analyzer, and the C concentration was determined by CS-3000 analyzer. The nominal and measured chemical compositions are listed in Table 1. The ingot underwent homogenization at 1000 °C for 12 h and was then forged at 740 °C with a deformation of 75%. Finally, the forged samples were solution-treated at 900 °C for 30 min and water quenched. All heat treatments were carried out under high-purity argon atmosphere. The tensile samples with 2 × 8 × 1 mm gauge section were stretched on an Instron 5565 system using a video extensometer at a nominal strain rate

---

* Corresponding author. National Key Laboratory of Science and Technology on Materials Under Shock and Impact, School of Materials Science and Engineering, Beijing Institute of Technology, Beijing, 100081, China.
E-mail address: linyang@bit.edu.cn (L. Yang).

https://doi.org/10.1016/j.msea.2022.143355
Received 7 April 2022; Received in revised form 22 May 2022; Accepted 24 May 2022

Table 1

Nominal and measured chemical compositions of the alloy in wt.%.

Elements	Ti	Mo	Cr	Zr	C	N	O	H
Nominal	Bal.	6	3.5	1	–	–	–	–
Measured	Bal.	5.91	3.38	1.06	0.018	0.015	0.14	0.0052

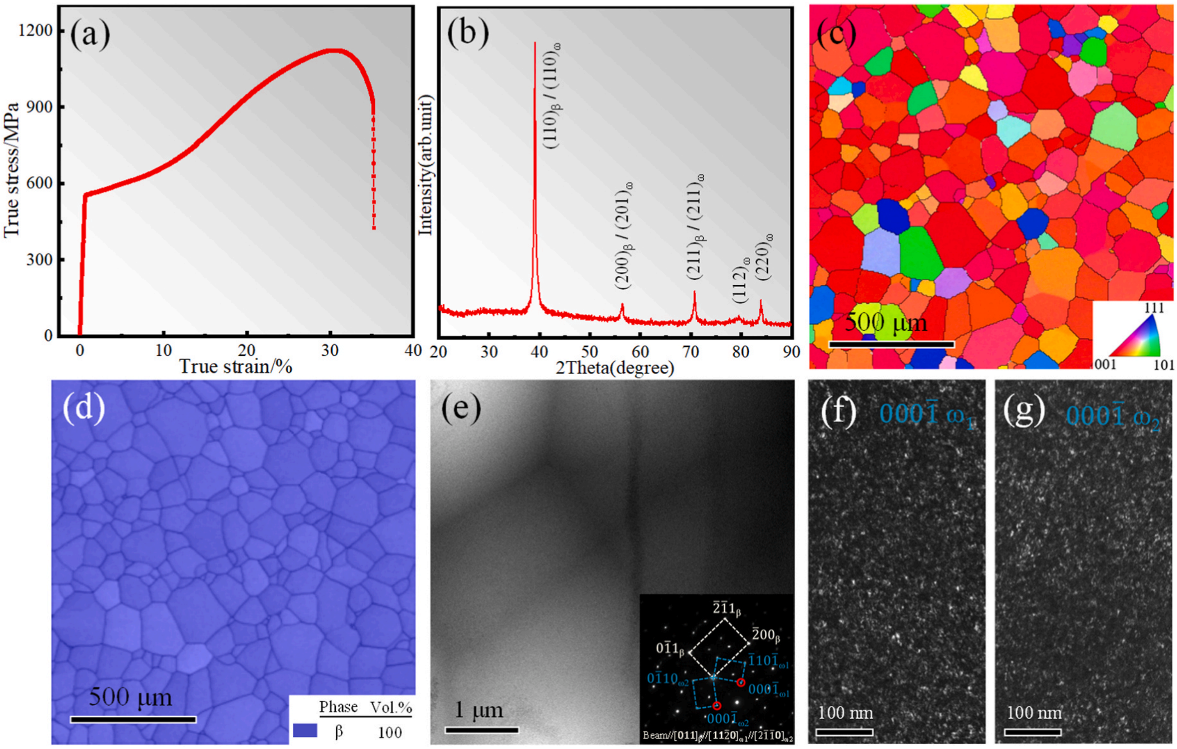

Fig. 1. Mechanical properties and microstructure analysis of the as-quenched alloy. (a) True stress-strain curve of the alloy stretched to failure. (b) XRD analysis. (c) EBSD IPF map. (d) EBSD phase map. (e) TEM bright-field image (The inset shows SAED pattern along the $[011]_\beta$ zone axis). (f–g) TEM dark-field images corresponding to the $[000\ \bar{1}]_{\omega1}$ and $[000\ \bar{1}]_{\omega2}$ reflections in SAED, respectively.

of $0.5 \times 10^{-3}\ s^{-1}$. The XRD tests were carried out using Bruker (2°/min, from 20°-90°; $\lambda_{Cu\alpha}$: 0.154 nm). The electron backscatter diffraction (EBSD) experiments were performed on a field emission gun scanning electron microscope (JSM 7200F) equipped with an EDAX velocity super probe. A FEI Themis Z transmission electron microscopy (TEM) with double-hexapole spherical-aberration corrector was used to observe the nano structures. To increase the efficiency of the computation without losing the element information, the virtual crystal approximation (VCA) method was applied to calculate the density of states (DOS). Formation enthalpy (H_f) and cohesive energy (Ec) were calculated by using the CASTEP module of the Materials Studio software. The difference in total energy, maximum force, maximum stress and maximum displacement for geometry optimization were set to be 1×10^{-7} eV/atom, 0.01 eV/Å, 0.05 GPa, and 0.001 Å during the optimization calculation, respectively.

3. Results and discussion

The true stress-strain curve of the alloy stretched to failure is shown in Fig. 1a. The true ultimate tensile strength and elongation to failure are measured to be 1123 MPa and 35%, respectively. XRD result shows that the as-quenched alloy is composed of β and ω phases (Fig. 1b). EBSD inverse pole figure (IPF) map and phase map detect the existence of β phase and determine its average grain size of ~95 μm (Fig. 1c and d). However, further selected area electron diffraction (SAED) reveals the existence of two nanoscale athermal ω variants in the β matrix, which cannot be detected in TEM bright-field image due to its extremely small size (Fig. 1e and inset). The orientation relationship of athermal ω phases with the β matrix satisfies $[011]_\beta//[11\ \bar{2}\ 0]_{\omega1}//[2\ \bar{1}\bar{1}\ 0]_{\omega2}$. The TEM dark-field (DF) images corresponding to $[000\ \bar{1}]_{\omega1}$ and $[000\ \bar{1}]_{\omega2}$ reflections show that both variants are uniformly dispersed in β matrix, with particle diameters less than 10 nm (Fig. 1f and g).

The true stress-strain curve of the alloy stretched up to 1.5% strain is shown in Fig. 2a. The 0.2% offset yield stress ($\sigma_{0.2}$) is 588 MPa. The stress at 1.5% strain is 630 MPa, which is 7% higher than the $\sigma_{0.2}$. This indicates that the material undergoes strain hardening. Both EBSD IPF map (Fig. 2b) and TEM BF image (Fig. 2d) detect the appearance of band structures. Combining the EBSD phase map (Fig. 2c) and SAED patterns corresponding to the matrix region (S1) and the band region (S2) (Fig. 2e and f), the band structure is identified as ω phase, which is induced by the external stress. In addition, the volume fraction of SIω is determined by EBSD phase map to be 4.64%. The SAED spots of SIω overlaps with those of the athermal ω_1 variant that pre-exists in the matrix. The TEM DF images of the ω_1 and ω_2 variants reveal that the interior region in the band contains more ω_1 variants than that in the matrix, but no ω_2 variants are observed inside the bands (Fig. 2g and h). Composition analysis of the rectangular region (interface between the SIω and β matrix) in Fig. 2d shows that there is no elemental segregation (Fig. 2i). It is proved that the initial SIω bands is only formed by stress-induced atomic shear rather than by temperature-driven atomic diffusion. The schematic diagram of the atomic shear process of β→ω phase transformation is shown in Fig. 2j [23]. The A and B atoms in β phase are shifted by 1/12[111] to the A′ and B’, respectively, forming a unit cell of

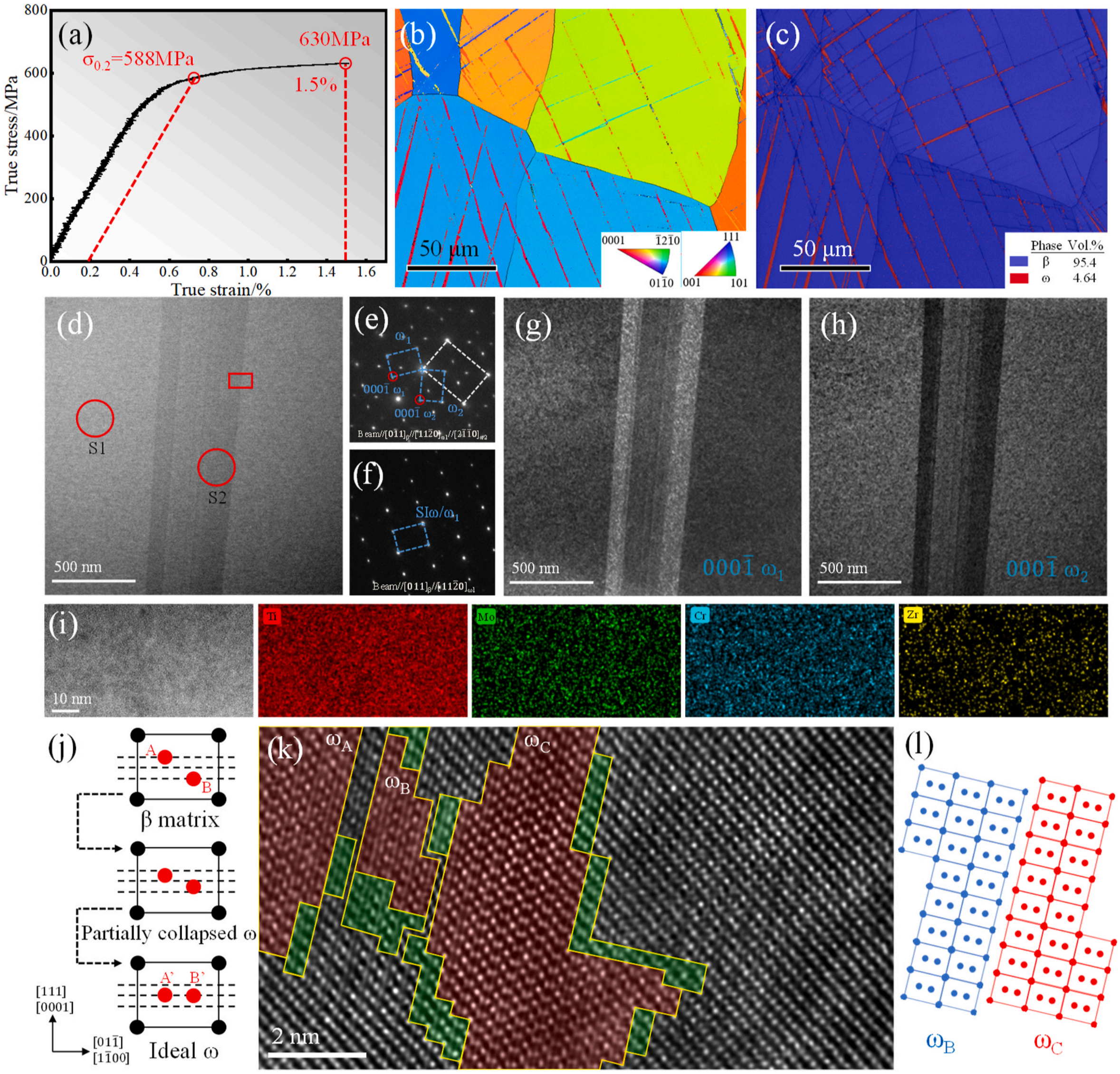

Fig. 2. Microstructure analysis of the alloy at 1.5% strain. (a) True stress-strain curve. (b) EBSD IPF map. (c) EBSD phase map. (d) TEM bright-field image. (e–f) SAED patterns recorded from the S1 and S2 areas in (d), respectively. (g–h) TEM dark-field images of ω_1 and ω_2 variants using the reflections of $(000\bar{1})_{\omega1}$ and $(000\bar{1})_{\omega2}$ in (e), respectively. (i) TEM mapping images of each element (Ti, Mo, Cr and Zr) at β/ω interface. (j) Schematic diagram of the atomic shear process of β→ω phase transformation. (k) High-resolution TEM image of the interface between the stress-induced ω band and the β matrix. (l) Schematic diagram of the atomic arrangement at the interface between ω_B and ω_C particles in (k).

the hexagonal ω phase, while a partially collapsed trigonal ω phase lattice is formed when the shear distance is between 0 and 1/12[111]. The atomic arrangement at the SIω/β interface along the $[011]_\beta$ axis is shown in Fig. 2k, where the SIω band is on the left and the β matrix is on the right. Three hexagonal ω_1 variant particles (marked as ω_A, ω_B and ω_C, highlighted in red) are observed inside the band. There are a few partially collapsed trigonal ω structures (highlighted by green) and untransformed β matrix between the particles. In addition, the interface of ω_B/ω_C shows the chaotic arrangement of atoms, which is caused by the coalescence of the growing interface of the two particles, as shown in the schematic diagram (Fig. 2l). Therefore, it can be concluded that the initial formation of the SIω bands is related to the growth and coalescence of the single athermal ω variant pre-existing in the matrix.

The true stress-strain curve of the alloy at a tensile strain of 5% is shown in Fig. 3a. The stresses at 1.5% strain and 5% strain are 639 MPa and 688 MPa, respectively, indicating further hardening of the material. EBSD IPF map (Fig. 3b) and phase map (Fig. 3c) show that the volume fraction of the SIω bands at 5% strain is 33.5%, which is significantly higher than that at 1.5% strain. This indicates the continued occurrence of the β→SIω phase transformation as the strain accumulates. Interestingly, TEM observations show that a series of fine lamellar structures appear inside the initial ω bands (Fig. 3d). SAED pattern implies the existence of α phase in the lamellar region (Fig. 3d inset). Furthermore, the high-resolution atomic image also shows the existence of β phase in the lamellar structure, whose orientation relationship with the α phase satisfies $[011]_\beta//[0001]_\alpha$ (Fig. 3e and f). The interface between the two phases exhibits a stepped feature, as shown by the yellow dotted line in Fig. 3f. Compared with the α-layer, the width of the β-layer is very small, so the diffraction characteristic associated with the corresponding β phase is not obvious in the SAED pattern. These results prove that the lamellar structure is formed by the SIω→α+β phase transformation. Fig. 3g shows the distribution characteristics of the elements of Ti, Cr, Mo and Zr in the α/β lamellar region. The content of Ti in the α lamellar is high while the contents of Cr and Mo are low with the opposite trend shown in the β lamellar. As a neutral element, the content of Zr exhibits a uniform distribution. This demonstrates the occurrence of elemental

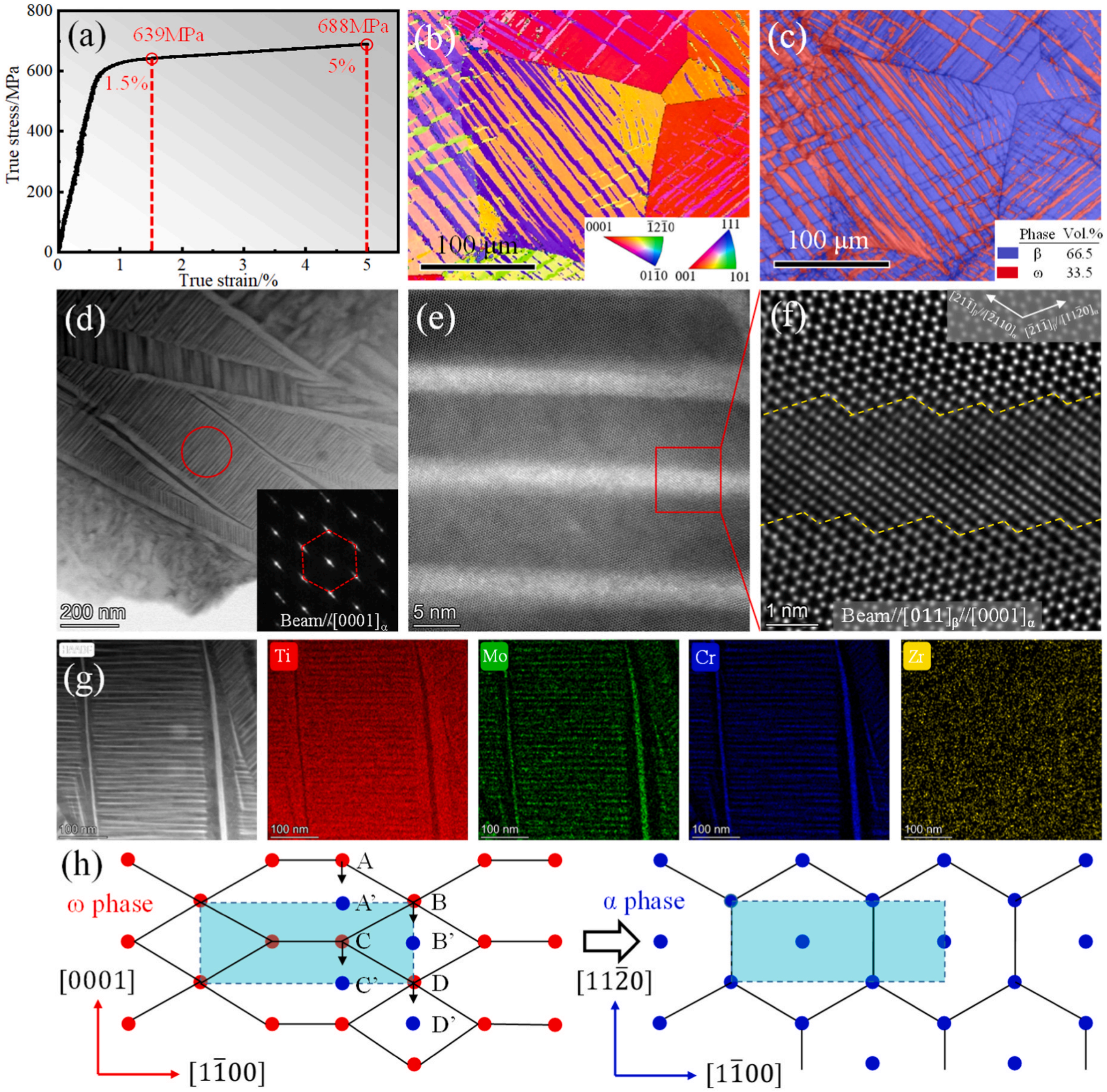

Fig. 3. Microstructure analysis of the alloy at 5% strain. (a) True stress-strain curve. (b) EBSD IPF map. (c) EBSD phase map. (d) TEM bright-field image (inset shows the SAED pattern recorded from the circled area). (e–f) High-resolution TEM image of the lamellar area. (g) TEM mapping images of each element (Ti, Mo, Cr and Zr) corresponding to the lamellar area. (h) Schematic diagram of the atomic shear process of ω→α phase transformation.

diffusion during stretching. Unlike the common thermal diffusion process, the quasi-static tensile process at room temperature excludes the influence of thermal effect. The diffusion force is provided by the accumulation of stress in the initial band structure, which is similar with the stress-induced diffusion phenomenon reported in other alloys [24–28]. Therefore, the SIω→α+β phase transformation exhibits both characteristics resulting from elements diffusion and atomic shear. The atomic shear path of SIω→β corresponds to the reverse process in Fig. 2j. The atomic shear path of SIω→α is shown in Fig. 3h [29]. The A, B, C and D atoms on the $(11\bar{2}0)_\omega$ plane move 1.48 Å to the A′, B′, C′ and D’ positions, respectively. An expansion of ~4.7% along [0001] and a shrinkage of ~4.5% along $[1\bar{1}00]$ leads to the formation of α unit cell. The orientation relationship between ω and α phases is $(0001)_\alpha//(11\bar{2}0)_\omega$, $[11\bar{2}0]_\alpha//[0001]_\omega$.

The TEM energy-dispersive X-ray spectroscopy (EDS) line scan profile acquired across the lamellar structure shows the periodic composition modulation characteristic (Fig. 4a), which is related to the interphase distribution of α and β phases. The compositions of α and β in the lamellar region (α_b and β_b) obtained from Fig. 4a, together with the compositions of matrix β phase (β_0) and athermal ω/initial SIω phase (ω_0) are shown in Table 2. On the basis of the quantized compositions, the density of states (DOS) of these phases are analyzed (Fig. 4b). The DOS of β_0 shows that its fermi level is near the wave crest, indicating that the atoms are metallically bonded to each other. When the β_0 lattice collapses into an ω_0 lattice, a pseudogap appears at the fermi level, indicating that the atomic bonds exhibit covalent properties. As the ω_0 lattices transform into α_b phase lattices, the increase in depth and width of the pseudogap reveals the rise in the covalent bonds of the atoms, which eventually leads to the hardening of the material [30].

The driving force of the β→SIω→α+β phase transformation is evaluated by the formation enthalpy (H_f) and the cohesive energy (E_c):

$$H_f = \frac{1}{n}E_{tot} - aE^{Ti}_{solid} - bE^{Mo}_{solid} - cE^{Cr}_{solid} - dE^{Zr}_{solid} \qquad (1)$$

$$E_c = \frac{1}{n}E_{tot} - aE^{Ti}_{atom} - bE^{Mo}_{atom} - cE^{Cr}_{atom} - dE^{Zr}_{atom} \qquad (2)$$

where E_{tot} represents the total energy of the single phase; n is the number

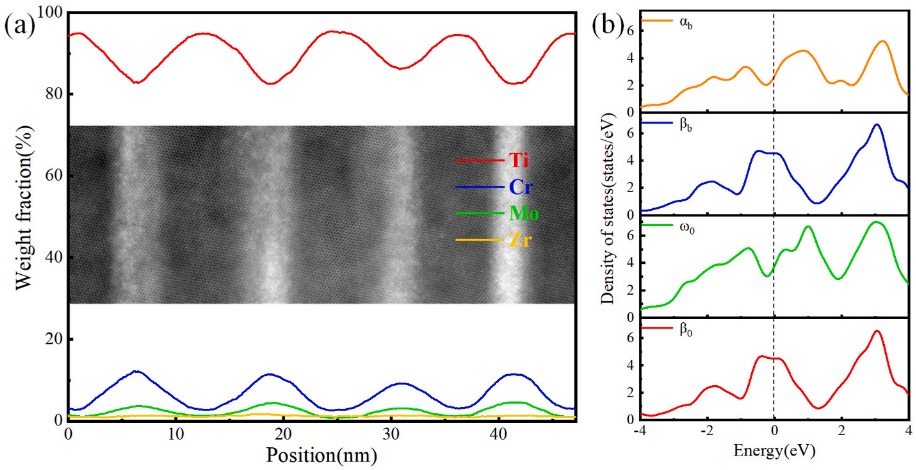

Fig. 4. Composition and density of states analysis of the stress-induced phases. (a) TEM EDS line scanning analysis along the lamellar structure. (b) DOS maps of the β_0, ω_0, α_b and β_b.

Table 2
The compositions of β_0, ω_0, α_b and β_b phases (at. %).

Element	Ti	Cr	Mo	Zr
β_0	93.127	3.232	3.063	0.578
ω_0	93.127	3.232	3.063	0.578
β_b	85.886	11.547	1.888	0.679
α_b	96.16	2.644	0.608	0.588

Table 3
Lattice constant (after geometrical optimization), formation enthalpy and cohesive energy of β_0、ω_0、α_b and β_b.

Phase	Space group	*a*/Å	*b*/Å	*c*/Å	H_f (eV·atom^{-1})	E_c (eV·atom^{-1})
β_0	229 ($Im\bar{3}m$)	3.218	3.218	3.218	−8.23	−14.86
ω_0	191 ($P6/mmm$)	4.552	4.552	2.775	−8.31	−15.48
β_b	229 ($Im\bar{3}m$)	3.156	3.156	3.156	−8.06	−14.75
α_b	194 ($P6_3/mmm$)	2.903	2.903	4.634	−2.01	−8.54

of atoms in a unit cell; E^i_{solid} is the energy per atom of element *i* in the solid state of the crystal structure; E^i_{atom} is the energy per atom of *i* under isolated state; *a*, *b*, *c* and *d* represent the atomic fraction of Ti, Mo, Cr and Zr in the alloy, respectively.

The calculation results of H_f, E_c and lattice constants for β_0、ω_0、α_b and β_b phases are listed in Table 3. The H_f and E_c of the ω_0 are lower than those of the β_0 phase, so the athermal ω phase can be precipitated from the matrix during the quenching process, and the stress-induced ω phase transformation can occur at a low stress. The H_f and E_c values of α_b and β_b are higher than ω_0, indicating that extra driving force is essential for the activation of SIω→α_b+β_b phase transformation such as the external loading. This is similar to the thermal-induced ω→β and ω→α phase transformations during the aging treatment [31,32].

4. Conclusion

In summary, a metastable β-type titanium alloy Ti–6Mo-3.5Cr–1Zr was developed in this work. At initial stage of plastic deformation, stress-induced ω (SIω) phase transformation dominates and its formation is accomplished by the localized growth and coalescence of single athermal ω variant pre-existing in the β matrix. As the strain increases, the generated SIω bands are transformed to α+β phase, undergoing sequential transformation associated with β→SIω→α+β. Density of states analysis shows that the covalent components in β phase, SIω phase, stress-induced α phase increase successively, which leads to the hardening of the material. The thermodynamic and kinetic mechanisms of the stress-induced β→ω→α+β phase transformation are revealed by the formation enthalpy and cohesive energy calculation and atomic shear analysis, respectively. This work will enrich us to understand the transformation mechanisms in metastable titanium alloys and can be used in materials design to simultaneously optimize the strength and plasticity.

Originality statement

I write on behalf of myself and all co-authors to confirm that the results reported in the manuscript are original and neither the entire work, nor any of its parts have been previously published. The authors confirm that the article has not been submitted to peer review, nor has been accepted for publishing in another journal. The authors confirm that the research in their work is original, and that all the data given in the article are real and authentic. If necessary, the article can be recalled, and errors corrected.

CRediT authorship contribution statement

Kai Chen: Methodology, Investigation, Formal analysis, Writing. **Qunbo Fan:** Methodology, Supervision, Funding acquisition. **Lin Yang:** Review, Funding acquisition. **Shun Xu:** Review, Funding acquisition. **Jiahao Yao:** Review. **Yu Gao:** Review. **Wei Lei:** Review.

Declaration of competing interest

The authors declare that they have no known competing financial interests or personal relationships that could have appeared to influence the work reported in this paper.

Acknowledgements

The authors are grateful to the financial support from the Natural Science Foundation of China (Grant No. 51901102) and Natural Science Foundation of China (Grant No. 52101005).

References

[1] P.D. Frost, W.M. Parris, L.L. Hirsch, J.R. Doig, C.M. Schwartz, Isothermal transformation of titanium-chromium alloys, Trans. ASM. 46 (1954) 231–256.

[2] D. de Fontaine, O. Buck, A Monte Carlo simulation of the omega phase transformation, Philos. Mag. A 27 (1973) 967–983.

[3] A. Devaraj, S. Nag, R. Srinivasan, R.E.A. Williams, S. Banerjee, R. Banerjee, H. L. Fraser, Experimental evidence of concurrent compositional and structural instabilities leading to ω precipitation in titanium-molybdenum alloys, Acta Mater. 60 (2012) 596–609.

[4] C. Li, G. Yin, A. Zhang, Y. Zhao, Q. Li, Simple models to account for the formation and decomposition of athermal ω phase in titanium alloys, Scripta Mater. 117 (2016) 28–31.

[5] C. Li, S. Huang, G. Yin, A. Zhang, Z. Zhao, Y. Zhao, A simple model to ascertain the initial formation concentration of athermal ω phase in titanium alloys, Comput. Mater. Sci. 123 (2016) 263–267.

[6] J. Nejezchlebová, M. Janovská, H. Seiner, P. Sedlák, M. Landa, J. Šmilauerovác, J. Stráský, P. Harcuba, M. Janeček, The effect of athermal and isothermal ω phase particles on elasticity of β-Ti single crystals, Acta Mater. 110 (2016) 185–191.

[7] H. Liu, M. Niinomi, M. Nakai, K. Cho, Athermal and deformation-induced ω-phase transformations in biomedical beta-type alloy Ti-9Cr-0.2O, Acta Mater. 106 (2016) 162–170.

[8] W. Chen, K. Li, G. Yu, J. Ren, Y. Zha, J. Sun, Deformation twinning-induced single-variant ω-plates in metastable β-Ti alloys containing athermal ω-precipitates, J. Mater. Sci. 56 (2021) 7710–7726.

[9] J.C. Williams, B.S. Hickman, H.L. Marcus, The effect of omega phase on the mechanical properties of titanium alloys, Metall. Trans. A 2 (1971) 1913–1919.

[10] A.W. Bowen, Omega phase embrittlement in aged Ti-15%Mo, Scripta Mater. 5 (1971) 709–716.

[11] M.J. Lai, C.C. Tasan, D. Raabe, Deformation mechanism of ω-enriched Ti-Nb-based gum metal: dislocation channeling and deformation induced ω-β transformation, Acta Mater. 100 (2015) 290–300.

[12] B. He, J. Li, X. Cheng, H. Wang, Brittle fracture behavior of a laser additive manufactured near-β titanium alloy after low temperature aging, Mater. Sci. Eng. 699 (2017) 229–238.

[13] R. Dong, J. Li, H. Kou, J. Fan, Y. Zhao, H. Hou, L. Wu, ω-Assisted refinement of α phase and its effect on the tensile properties of a near β titanium alloy, J. Mater. Sci. Technol. 44 (2020) 24–30.

[14] N.G. Jones, R.J. Dashwood, M. Jackson, D. Dye, β Phase decomposition in Ti-5Al-5Mo-5V-3Cr, Acta Mater. 57 (2009) 3830–3839.

[15] H.P. Ng, E. Douguet, C.J. Bettles, B.C. Muddle, Age-hardening behaviour of two metastable beta-titanium alloys, Mater. Sci. Eng. 527 (2010) 7017–7026.

[16] X.L. Wang, L. Li, W. Mei, W.L. Wang, J. Sun, Dependence of stress-induced omega transition and mechanical twinning on phase stability in metastable β Ti-V alloys, Mater. Char. 107 (2015) 149–155.

[17] T.S. Kuan, R.R. Ahrens, S.L. Sass, The stress-induced omega phase transformation in Ti-V alloys, Metall. Trans. A 6 (1975) 1767–1774.

[18] X.L. Wang, L. Li, H. Xing, P. Ou, J. Sun, Role of oxygen in stress-induced ω phase transformation and {332}<113> mechanical twinning in β Ti-20V alloy, Scripta Mater. 96 (2015) 37–40.

[19] S.Q. Wu, D.H. Ping, Y. Yamabe-Mitarai, W.L. Xiao, Y. Yang, Q.M. Hu, G.P. Li, R. Yang, {112}<111> Twinning during ω to body-centered cubic transition, Acta Mater. 62 (2014) 122–128.

[20] L. Li, W. Mei, H. Xing, X.L. Wang, J. Sun, Zigzag configuration of mechanical twin and stress-induced omega phase in metastable β Ti-34Nb (at.%) alloy, J. Alloys Compd. 625 (2015) 188–192.

[21] M. Morinaga, N. Yukawa, H. Adachi, Theory of the d electrons alloy design, J. Iron and Steel Inst. 71 (1985) 1441–1451.

[22] M. Abdel-Hady, K. Hinoshita, M. Morinaga, General approach to phase stability and elastic properties of β-type Ti-alloys using electronic parameters, Scripta Mater. 55 (2006) 477–480.

[23] S.K. Sikka, Y.K. Vohra, R. Chidambaram, Omega phase in materials, Prog. Mater. Sci. 27 (1982) 245–310.

[24] J.R. Spingarn, W.D. Nix, Diffusional creep and diffusionally accommodated grain rearrangement, Acta Metall. 26 (1978) 1389–1398.

[25] A. Galdikas, T. Moskalioviene, Modeling of stress induced nitrogen diffusion in nitrided stainless steel, Surf. Coating. Technol. 205 (2011) 3742–3746.

[26] T. Garnier, V.R. Manga, D.R. Trinkle, M. Nastar, P. Bellon, Stress-induced anisotropic diffusion in alloys: complex Si solute flow near a dislocation core in Ni, Phys. Rev. B 88 (2013) 134108.

[27] J. Koike, Y. Shimoyama, I. Ohnuma, T. Okamura, R. Kainuma, K. Ishida, K. Maruyama, Stress-induced phase transformation during superplastic deformation in two-phase Ti-Al-Fe alloy, Acta Mater. 48 (2000) 2059–2069.

[28] X. Zhu, Q. Fan, D. Wang, H. Gong, Y. Gao, F. Qian, S. Jin, G. Sha, A new dynamic recrystallization mechanism in adiabatic shear band of an α/β dual phase titanium alloy: composition redistribution, Scripta Mater. 206 (2022) 114229.

[29] A. Rabinkin, M. Talianker, O. Botstein, Crystallography and a model of the α→ ω phase transformation in zirconium, Acta Mater. 29 (1981) 691–698.

[30] W. Chen, S. Cao, W. Kou, J. Zhang, Y. Wang, Y. Zha, Y. Pan, Q. Hu, Q. Sun, J. Sun, Origin of the ductile-to-brittle transition of metastable β-titanium alloys: self-hardening of ω-precipitates, Acta Mater. 170 (2019) 187–204.

[31] D. Li, W. Wan, L. Zhu, Y. Jiang, S. Shao, G. Yang, H. Liu, D. Yi, S. Cao, Q. Hu, Experimental and DFT characterization of interphase boundaries in titanium and the implications for ω-assisted α phase precipitation, Acta Mater. 151 (2018) 406–415.

[32] V.I. Zel'dovich, N.Y. Frolova, A.M. Patselov, V.M. Gundyrev, A.E. Kheifets, V. P. Pilyugin, The ω-phase formation in titanium upon deformation under pressure, Phys. Met. Metallogr. 109 (2010) 30–38.